

Article

# Ocean Wave Active Compensation Analysis for Redundant Hybrid Boarding System: A Multi-Task Motion Planning Method

Yueyue Wang <sup>1</sup>, Yanhui Wei <sup>1,2,\*</sup> , Weihang Gao <sup>3</sup>, Tianyu Ma <sup>1</sup> and Yuntao Han <sup>1,2</sup>

<sup>1</sup> College of Intelligent Systems Science and Engineering, Harbin Engineering University, Harbin 150001, China; wangyueyue@hrbeu.edu.cn (Y.W.)

<sup>2</sup> Nanhai Innovation and Development Center, Harbin Engineering University, Sanya 572000, China

<sup>3</sup> Key Laboratory of Earthquake Engineering and Engineering Vibration, Institute of Engineering Mechanics, China Earthquake Administration, Harbin 150001, China; gaoweihang@iem.ac.cn

\* Correspondence: wyheauini@hrbeu.edu.cn

**Abstract:** In this paper, to effectively solve the joint motion planning of a nine-DOF redundant hybrid boarding system in the process of ocean wave active compensation, we present a multi-task motion planning (MTMP) method for the redundant hybrid boarding system. First, the hybrid mechanism is disassembled into a six-DOF parallel mechanism and a three-DOF serial mechanism for kinematic analysis separately to obtain the Jacobian matrix of the hybrid mechanism in the task space. Then, according to the configuration characteristics of the hybrid mechanism and to avoid the defects of the pseudo-inverse and weighted pseudo-inverse methods in motion planning, several secondary tasks are proposed to constrain the motion planning of the hybrid mechanism. Based on simulations and comparisons, the results show that the MTMP method solves the problems of joint limitation, reverse compensation, overlap compensation, and divergence with time in the motion planning of the pseudo-inverse method and the weighted pseudo-inverse method. Meanwhile, the MTMP method has more superiority in the joint margin and compensation space range.

**Keywords:** hybrid mechanism; multi-task; motion planning; wave compensation



**Citation:** Wang, Y.; Wei, Y.; Gao, W.; Ma, T.; Han, Y. Ocean Wave Active Compensation Analysis for Redundant Hybrid Boarding System: A Multi-Task Motion Planning Method. *J. Mar. Sci. Eng.* **2023**, *11*, 708. <https://doi.org/10.3390/jmse11040708>

Academic Editors: Mai The Vu and Hyeung-Sik Choi

Received: 20 February 2023

Revised: 18 March 2023

Accepted: 20 March 2023

Published: 25 March 2023



**Copyright:** © 2023 by the authors. Licensee MDPI, Basel, Switzerland. This article is an open access article distributed under the terms and conditions of the Creative Commons Attribution (CC BY) license (<https://creativecommons.org/licenses/by/4.0/>).

## 1. Introduction

The International Renewable Energy Agency's analysis indicated that an increase in cumulative installed offshore wind capacity from 34 GW in 2020 to 380 GW and to more than 2000 GW by 2050 could be employed globally [1]. With the construction of offshore wind farms, the scale of offshore wind power investment and subsequent Operation and Maintenance (O&M) will increase rapidly [2]. During the O&M of offshore wind power, personnel and equipment need to be transferred across platforms, due to the harsh marine environment of offshore wind farms [3]. The relative poses of different platforms fluctuate considerably because of the waves, which causes the O&M vessels to be unable to dock. Not only is this dangerous for the operating personnel, but it also causes collisions between O&M vessels and wind power platforms, resulting in severe maritime safety accidents. Therefore, a wave-compensated boarding system is needed to ensure the fast and safe cross-boarding of personnel and equipment.

Compared with the offshore motion compensation crane [4–6], the boarding system is more suitable for cross-platform O&M personnel. With the development of wave compensation boarding system technology, there are different types of boarding systems. The three-DOF serial gangway is the most common and widely used [7–9], as shown in Figure 1. In existing research on the configuration of the wave compensation system [10,11], the serial configuration has a large compensation range for the position space. However, it cannot achieve complete position and orientation coupling compensation. The parallel

configuration is more advantageous than the orientation compensation space, and the position–orientation coupling compensation is realized in a small area. However, the motion compensation space of the parallel configuration is limited, and complete compensation is impossible in a high-sea state. Therefore, a hybrid mechanism with both a serial configuration and a parallel configuration has appeared [12]. However, the hybrid mechanism with few degrees of freedom cannot achieve motion compensation with full degrees of freedom in a large space. A large-scale hybrid boarding system with redundant degrees of freedom is required in severe and complex sea conditions.



**Figure 1.** The three-DOF serial gangway.

Taking into account the characteristics of different structures in wave compensation, this paper uses a combination of the six-DOF Stewart parallel configuration and the three-DOF serial configuration to design a hybrid wave compensation system with a nine-DOF redundant mechanism. Meanwhile, considering the configuration characteristics of the hybrid mechanism, reasonable motion planning processing is essential for redundant mechanisms. For redundant mechanism motion planning problems, Sun et al. [13] proposed a hybrid mechanism composed of a five-DOF parallel mechanism and a three-DOF serial mechanism. The parallel mechanism was transformed into a serial configuration and a three-DOF serial configuration to form a multi-DOF serial mechanism in the motion planning process. They carried out a kinematic analysis of the newly composed multi-DOF serial mechanism. Su et al. [14] presented a novel RNN-based approach to facilitate accurate task tracking based on the general quadratic performance index, which included simultaneously managing the constraints on the remote center of motion joint angle and joint velocity. Zhang et al. [15,16] proposed a novel varying-parameter recurrent neural network (called the varying-parameter convergent–differential neural network (VP-CDNN)) to solve non-repetitive problems of redundant robot manipulators and came up with a CCNC-QP-DNN to solve the redundancy resolution problems that effectively extended the solution set space. Wang et al. [17] made a seven-DOF serial–parallel hybrid humanoid robotic arm. A path with a better joint-rate distribution was gained based on the normalized Jacobian condition number to avoid abrupt joint angle changes. Travel time, energy consumption, and torque fluctuations were also considered. Peng et al. [18] propounded an end-effector pose and arm-shape synchronous planning method for a hyper-redundant manipulator passing through space narrow parallel slits based on extended Jacobian matrix redundancy decomposition. Lee et al. [19] used task-priority motion planning control for a redundant rescue robot. The main task allocation strategies included end-effector operation, waist posture and lower-arm level motion, center gravity balancing, and joint limit avoidance.

For the above motion planning method, the virtue of the configuration simplification method is that the calculation is simple, but the problem is that not all configurations are applicable. The neural network motion planning method can solve the nonlinear problem in the kinematics solution process, but its shortcoming is a large amount of calculation. The motion planning method based on internal configuration can fully consider the advantages and disadvantages of the internal configuration of redundant mechanisms and can improve the accuracy and effectiveness of motion planning.

In order to solve the joint motion planning problem efficiently, a motion planning method for the nine-DOF redundant hybrid active compensation boarding system is proposed. Motion constraints are performed by analyzing the conformational characteristics of the internal configuration. This approach ensures redundant mechanism end-effector trajectory tracking while achieving proper motion planning. The redundant hybrid boarding system is referred to as a hybrid mechanism. Section 2 introduces the model parameters of the hybrid mechanism. In Section 3, we model the kinematics of the hybrid mechanism, and the Jacobian matrix of the hybrid mechanism is obtained by mechanism disassembly and split modeling. Section 4 introduces the MTMP method. The pseudo-inverse and weighted pseudo-inverse methods are compared with the MTMP method for simulation in Section 5.

## 2. System Description

### 2.1. Hybrid Mechanism Design

The hybrid mechanism design should take into account wave motion variation. Sometimes, the hydrodynamic coupling of a wind turbine and O&M vessel is also considered [20]. The hybrid mechanism detects the changes in the position and orientation of the O&M vessel to compensate accordingly, ensuring that personnel carry equipment reach the offshore operating platform safely and steadily. The hybrid mechanism can be installed in the middle or stern of the vessel. When the end-effector comes to the target point, the hybrid mechanism enters the motion compensation mode.

The hybrid mechanism comprises a nine-DOF hydraulic control system, which contains three parts: motion platform subsystem, motion control subsystem, and hydraulic power subsystem. The motion platform subsystem is composed of a six-DOF parallel mechanism and a connected three-DOF serial mechanism. The parallel mechanism consists of one mobile platform, six servo-hydraulic cylinders, twelve Hooke joints, and six hinged supports. The serial mechanism consists of one slewing ring, two luffing cylinders, and one telescopic gangway. The structural diagram of the motion platform subsystem of the hybrid mechanism is shown in Figure 2. The motion control subsystem consists of an operator console, motion control computer, motion servo control software, motion simulation software, motion control modules (boards), signal conditioning modules, and other logic control devices and logic control circuits. The hydraulic power subsystem consists of a hydraulic pump station, electricity control cabinet, etc.

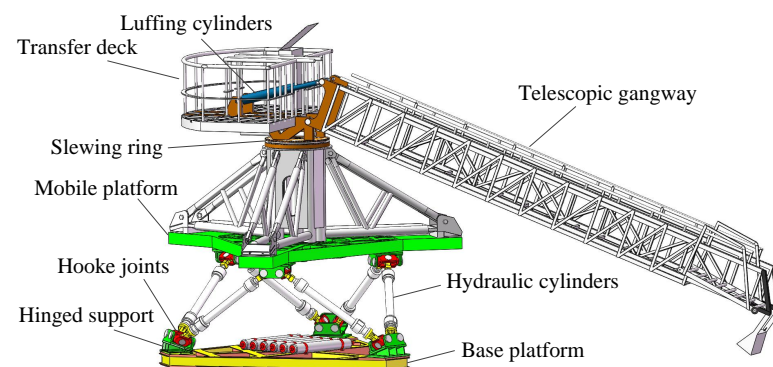


**Figure 2.** Structural diagram of the hybrid mechanism.

The hybrid mechanism motion platform subsystem has the merits of the high stiffness and high load capacity of the parallel mechanism [21,22], which make it suitable to compensate for the six-DOF position and orientation variation in the O&M vessel [23]. Meanwhile, it also has the benefit of the extensive working range of the serial mechanism. Through the serial-parallel combination, the hybrid mechanism has better robustness and larger motion compensation space [24,25]. Since the hybrid mechanism is a nine-DOF redundant configuration, its internal motion planning has a certain degree of complexity.

### 2.2. Dimensions and Parameters

The main parameters of the motion platform subsystem of the hybrid mechanism are shown in the following. Figure 3 is a side view of the motion platform of the hybrid mechanism, Figure 4 is a top view of the parallel mechanism, and Table 1 provides the main dimensional parameters of the hybrid mechanism.

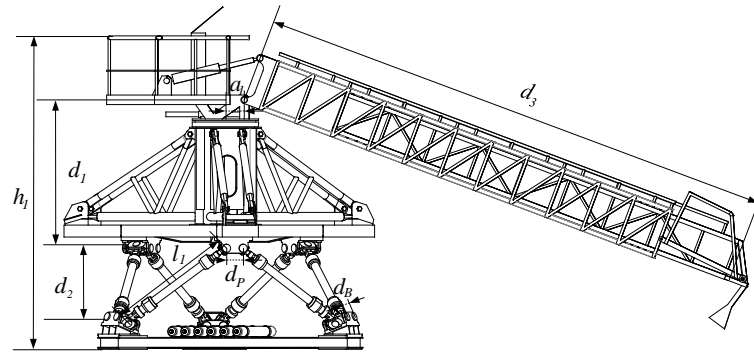


Figure 3. Side view of the hybrid mechanism.

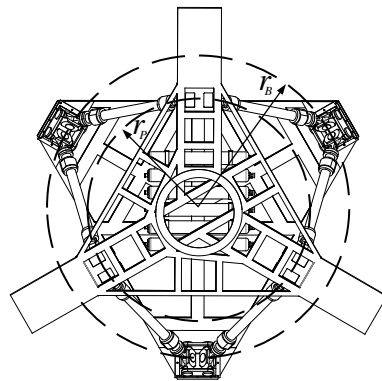


Figure 4. Top view of the parallel mechanism.

Table 1. Parameters of the hybrid mechanism.

Parameter	Description	Value	Unit
$h_1$	Total height	6.482	m
$d_1$	Height from top hinge circle to transfer deck	3.106	m
$d_2$	Height from bottom hinge circle to top hinge circle	1.525–3.595	m
$d_3$	Length of the gangway	9.552–16.552	m
$l_1$	Length of parallel mechanism leg	2.580–4.180	m
$a_1$	Deviation between swing axis and central axis	0.230	m
$d_B$	Distance between bottom hinge points	0.350	m
$d_P$	Distance between top hinge points	0.350	m
$r_B$	Radius of bottom hinge circle	2.650	m
$r_P$	Radius of top hinge circle	1.950	m

### 3. Kinematics

#### 3.1. Reference Frames

According to the configuration characteristics of the hybrid mechanism, it can be disassembled into two parts, a six-DOF parallel mechanism and a three-DOF serial mechanism, and a coordinate system is established. Firstly, the base frame  $O_B - x_b y_b z_b$  and mobile platform frame  $O_P - x_p y_p z_p$  of the parallel mechanism are established on the center points of the top and bottom hinge circles, respectively. Secondly, the frames of the serial mechanism are established. Since the second joint of the serial mechanism has two luffing

hydraulic cylinders, characterized as a swing joint for the hybrid mechanism, the second joint is used as a swing joint for modeling convenience. The frame  $O_p - x_p y_p z_p$  of the platform on the parallel mechanism is used as the base frame  $O_0 - x_0 y_0 z_0$  of the serial mechanism. The joint frames of the serial mechanism are the first slewing joint frame  $O_1 - x_1 y_1 z_1$ , the second swing joint frame  $O_2 - x_2 y_2 z_2$ , and the third telescopic joint frame  $O_3 - x_3 y_3 z_3$ . The inertial frame, the vessel frame, the sensor frame, the base frame of the hybrid mechanism, and the end-effector frame of the hybrid mechanism are established for the operational task of the hybrid mechanism, as shown in Figure 5.

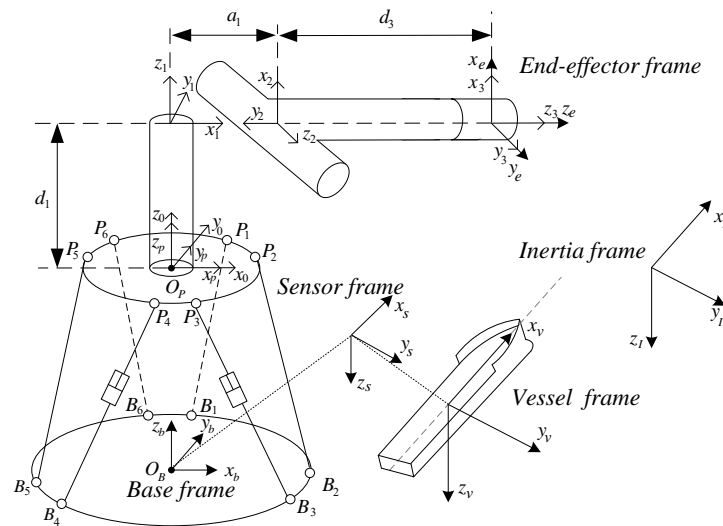


Figure 5. Kinematic frame of the hybrid mechanism.

**Inertial frame:** The inertial reference frame is a reference frame that is stationary or moves in a straight line at a constant velocity in absolute space.

**Vessel frame:** The vessel frame is established under the standard motion of the vessel. The x-direction is along the vessel’s midline from stern to bow, the y-direction points to starboard, and the z-direction points to the vessel’s bottom. The vessel frame is fixed to the center of the vessel and follows the movement of the vessel [26].

**Sensor frame:** The sensor is placed on the base of the parallel mechanism. Therefore, the sensor frame is established at the origin of the base platform frame of the parallel mechanism. Since the sensor aims to measure the vessel’s movement, the sensor’s frame axis direction is consistent with the vessel coordinate frame system direction.

**Base frame:** The base frame of the hybrid mechanism and the frame of the parallel mechanism are the same. In the working state of sea wave compensation, the direction of the gangway is perpendicular to the heading direction of the vessel, so the x-direction of the hybrid mechanism is the y-direction of the sensor frame, and the y-direction of the hybrid mechanism is the x-direction of the sensor frame.

**End-effector frame:** The end frame of the hybrid mechanism is the same as the third joint frame of the serial mechanism.

### 3.2. Kinematics Analysis of Parallel Mechanism

The position vector and orientation vector of the mobile platform of the parallel mechanism in the base frame are defined as  $\eta_1 = [x_p, y_p, z_p]^T$  and  $\eta_2 = [\phi_p, \theta_p, \psi_p]^T$ , respectively. Then, the generalized six-DOF motion of the mobile frame is defined as  $\eta_p = [\eta_1^T, \eta_2^T]^T$ . The upper-right corner marker T indicates the transposition of matrices and vectors.

From the parallel mechanism diagram in Figure 6, it can be seen that each hinge point has symmetry on the frame axis.

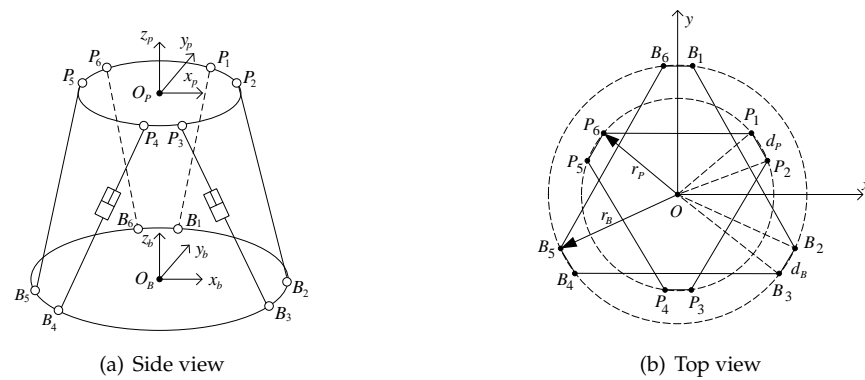


Figure 6. The six-DOF parallel platform.

The position vector of each hinge point  ${}^P P_i$  of the mobile platform and each hinge point  ${}^B B_i$  of the base platform can be expressed as

$${}^P P_i = [ r_p \cos \vartheta_{P_i} \quad r_p \sin \vartheta_{P_i} \quad 0 ]^T \tag{1}$$

$${}^B B_i = [ r_B \cos \vartheta_{B_i} \quad r_B \sin \vartheta_{B_i} \quad 0 ]^T \tag{2}$$

where

$$\begin{aligned} \vartheta_P &= [ \vartheta_{P_1} \quad \vartheta_{P_2} \quad \vartheta_{P_3} \quad \vartheta_{P_4} \quad \vartheta_{P_5} \quad \vartheta_{P_6} ]^T \\ &= [ \frac{\pi}{6} + \alpha \quad \frac{\pi}{6} - \alpha \quad -\frac{\pi}{2} + \alpha \quad -\frac{\pi}{2} - \alpha \quad \frac{5\pi}{6} + \alpha \quad \frac{5\pi}{6} - \alpha ]^T \\ \vartheta_B &= [ \vartheta_{B_1} \quad \vartheta_{B_2} \quad \vartheta_{B_3} \quad \vartheta_{B_4} \quad \vartheta_{B_5} \quad \vartheta_{B_6} ]^T \\ &= [ \frac{\pi}{2} - \gamma \quad -\frac{\pi}{6} + \gamma \quad -\frac{\pi}{6} - \gamma \quad -\frac{5\pi}{6} + \gamma \quad -\frac{5\pi}{6} - \gamma \quad \frac{\pi}{2} + \gamma ]^T \\ \alpha &= \arcsin\left(\frac{d_P}{2r_P}\right) \\ \gamma &= \arcsin\left(\frac{d_B}{2r_B}\right) \end{aligned}$$

The rotation matrix of the mobile frame relative to the base platform frame can be written as

$${}^B R_P = \begin{bmatrix} c\psi_p c\theta_p & c\psi_p s\theta_p s\phi_p - s\psi_p c\phi_p & c\psi_p s\theta_p c\phi_p + s\psi_p s\phi_p \\ s\psi_p c\theta_p & s\psi_p s\theta_p s\phi_p + c\psi_p c\phi_p & s\psi_p s\theta_p c\phi_p - c\psi_p s\phi_p \\ -s\theta_p & c\theta_p s\phi_p & c\theta_p c\phi_p \end{bmatrix} \tag{3}$$

where  $c*$  and  $s*$  are  $\cos(*)$  and  $\sin(*)$ , respectively. The vector position of each hinge point of the mobile platform in the frame of the base platform can be expressed as

$${}^B P_i = {}^B R_P {}^P P_i + {}^B O_P \tag{4}$$

The vector of the leg length can be expressed as

$$l_i = {}^B P_i - {}^B B_i \quad i = 1, 2, 3, 4, 5, 6 \tag{5}$$

The unit vector of leg length can be calculated with  $n_i = \frac{l_i}{|l_i|}$ .

${}^B \dot{P}_p$  and  ${}^B w_p$  are defined as the linear velocity and angular velocity motion variables of the mobile platform of the parallel mechanism in the base frame, respectively. The linear velocity and angular velocity motion variables of the mobile platform of the parallel mechanism in the mobile frame can be defined as  ${}^P \dot{P}$  and  $w_p$ , respectively.

According to the definition of the rotation matrix, this is expressed as

$${}^B\omega_P = {}^B R_P \omega_P \tag{6}$$

$${}^B \dot{P}_P = {}^B R_P^P \dot{P} \tag{7}$$

The Jacobian matrix relationship between the mobile platform velocity of the parallel mechanism in the base frame and the telescopic velocity vector of six legs can be written as

$$\dot{i} = J_P \begin{bmatrix} {}^B \dot{P}_P \\ {}^B \omega_P \end{bmatrix} \tag{8}$$

with  $\dot{i} = [ \dot{l}_1 \ \dot{l}_2 \ \dot{l}_3 \ \dot{l}_4 \ \dot{l}_5 \ \dot{l}_6 ]^T$  and  $J_P = \begin{bmatrix} \mathbf{n}_1^T & ({}^B P_1 \times \mathbf{n}_1)^T \\ \vdots & \vdots \\ \mathbf{n}_6^T & ({}^B P_6 \times \mathbf{n}_6)^T \end{bmatrix}$ .

### 3.3. Kinematics Analysis of Serial Mechanism

Combined with Figure 7, the Denavit–Hartenberg (DH) parameters of the serial mechanism are established [27], as shown in Table 2.

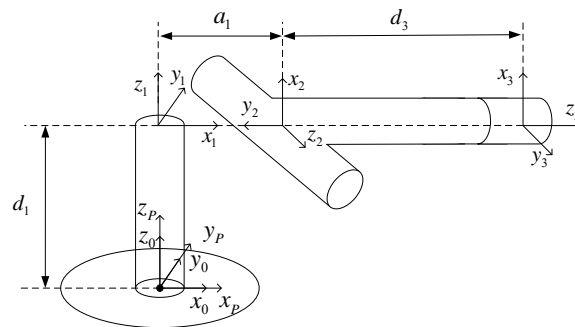


Figure 7. The three-DOF serial mechanism.

Table 2. DH parameters of the three-DOF serial mechanism.

$i$	$a_{i-1}$	$\alpha_{i-1}$	$d_i$	$\theta_i$
1	0	0°	$d_1$	$q_1$
2	$a_1$	90°	0	$q_2^*$
3	0	90°	$d_3^{**}$	0°

\*  $q_2$  offset is 90°. \*\*  $d_3$  offset is 9.552 m.

The parameters in Table 2 are brought into Equation (9) to find the transformation matrices  ${}^0T_1$ ,  ${}^1T_2$ , and  ${}^2T_3$  for each joint.

$${}^{i-1}T_i = \begin{bmatrix} cq_i & -sq_i & 0 & a_{i-1} \\ sq_i c\alpha_{i-1} & cq_i c\alpha_{i-1} & -s\alpha_{i-1} & -d_i s\alpha_{i-1} \\ sq_i s\alpha_{i-1} & cq_i s\alpha_{i-1} & c\alpha_{i-1} & d_i c\alpha_{i-1} \\ 0 & 0 & 0 & 1 \end{bmatrix} \tag{9}$$

The matrix  ${}^0T_3$  be expressed as

$${}^0T_3 = {}^0T_1 {}^1T_2 {}^2T_3 = \begin{bmatrix} n_x & o_x & a_x & p_x \\ n_y & o_y & a_y & p_y \\ n_z & o_z & a_z & p_z \\ 0 & 0 & 0 & 1 \end{bmatrix} \tag{10}$$

with  $n_x = c_1c_2, n_y = c_2s_1, n_z = s_2; o_x = s_1, o_y = -c_1, o_z = 0; a_x = c_1s_2, a_y = s_1s_2, a_z = -c_2; p_x = a_1c_1 + d_3c_1s_2, p_y = a_1s_1 + d_3s_1s_2, p_z = d_1 - d_3c_2$ , where  $s_1 = \sin q_1, s_2 = \sin q_2, c_1 = \cos q_1, c_2 = \cos q_2$ .

Using the vector product method, the Jacobian matrix  $J_{sp}$  of the linear velocity and the Jacobian matrix  $J_{so}$  of the angular velocity are obtained. The Jacobian matrix  $J_s$  is the end-effector velocity and the joint velocity of the serial mechanism.

$$J_s = \begin{bmatrix} J_{sp} \\ J_{so} \end{bmatrix} = \begin{bmatrix} -a_1s_1 - d_3s_1s_2 & d_3c_1c_2 & c_1s_2 \\ a_1c_1 + d_3c_1s_2 & d_3s_1c_2 & s_1s_2 \\ 0 & d_3s_2 & -c_2 \\ 0 & s_1 & 0 \\ 0 & -c_1 & 0 \\ 1 & 0 & 0 \end{bmatrix} \tag{11}$$

The Jacobian matrix of motion of the three-DOF serial mechanism can be written as

$$\dot{\zeta}_s = J_s \dot{q} \tag{12}$$

$\dot{\zeta}_s$  is the end-effector velocity of the serial mechanism, and  $\dot{q} = [ \dot{q}_1 \quad \dot{q}_2 \quad \dot{d}_3 ]^T$  is the joint velocity of the serial mechanism.

According to the definition of the generalized inverse, when the number of rows is greater than the number of columns, there is a left generalized inverse:

$$\dot{q} = J_s^+ \dot{\zeta}_s \tag{13}$$

where  $J_s^+ = (J_s^T J_s)^{-1} J_s^T$ .

### 3.4. Jacobian Matrix of Hybrid Mechanism in Task Space

The motion model of the hybrid mechanism is established in the task space. This is mainly used for research on joint motion planning algorithms. The velocity vector of the parallel mechanism's mobile platform and the serial mechanism's joint is defined as  $\dot{\zeta} = [ {}^P\dot{P} \quad w_P \quad \dot{q}_1 \quad \dot{q}_2 \quad \dot{d}_3 ]^T$ , and the end-effector velocity of the hybrid mechanism is defined as  $\dot{\zeta}_e = [ {}^B\dot{P}_E \quad {}^Bw_E ]$ .

The homogeneous transformation matrix of the hybrid mechanism from the end-effector frame to the base frame is expressed as Equation (14), which contains the position vector and the orientation matrix of the hybrid mechanism end-effector:

$${}^B T_E = \begin{bmatrix} {}^B R_P {}^P R_E & {}^B P_P + {}^B R_P {}^P P_E \\ 0 & 1 \end{bmatrix} \tag{14}$$

where  ${}^B R_P$  is the rotation matrix of the mobile frame in the parallel mechanism's base frame;  ${}^P R_E$  is rotation matrix of the serial mechanism's end-effector frame in the parallel mechanism's mobile frame;  ${}^B P_P$  is the position vector from the parallel mechanism's base frame to the mobile frame; and  ${}^P P_E$  is the position vector from the parallel mechanism's mobile frame to the serial mechanism's end-effector frame.

The position vector at the end of the hybrid mechanism can be written as

$${}^B P_E = {}^B P_P + {}^B R_P {}^P P_E \tag{15}$$

Derivatives on both sides of Equation (15) can be obtained as follows:

$${}^B \dot{P}_E = {}^B \dot{P}_P + {}^B \dot{R}_P {}^P P_E + {}^B R_P {}^P \dot{P}_E \tag{16}$$

According to the properties of the rotation matrix and the skew symmetry [27],  ${}^B\dot{\mathbf{R}}_P = S({}^B\mathbf{w}_P){}^B\mathbf{R}_P$ ,  $S(\mathbf{x})\mathbf{y} = -S(\mathbf{y})\mathbf{x}$ , and  $\mathbf{x} \times \mathbf{y} = -\mathbf{y} \times \mathbf{x}$  are known. Where  $S(\bullet)$  is the skew-symmetric matrix operator, Equation (16) can be expressed as

$${}^B\dot{\mathbf{P}}_E = {}^B\dot{\mathbf{P}}_P - S({}^B\mathbf{R}_P{}^P\mathbf{P}_E){}^B\mathbf{w}_P + {}^B\mathbf{R}_P{}^P\dot{\mathbf{P}}_E \tag{17}$$

$${}^B\dot{\mathbf{P}}_E = {}^B\dot{\mathbf{P}}_P - S({}^B\mathbf{R}_P{}^P\mathbf{P}_E){}^B\mathbf{w}_P + {}^B\mathbf{R}_P\mathbf{J}_{sp}\dot{\mathbf{q}} \tag{18}$$

The rotation matrix at the end of the hybrid mechanism can be written as

$${}^B\mathbf{R}_E = {}^B\mathbf{R}_P{}^P\mathbf{R}_E \tag{19}$$

Derivatives on both sides of Equation (19) are used to solve the orientation velocity matrix. According to the properties of the rotation matrix [27], given  $\dot{\mathbf{R}} = S(\mathbf{w})\mathbf{R}$ ,  $\mathbf{R}\mathbf{R}^T = \mathbf{R}^T\mathbf{R} = \mathbf{I}$  and  $\mathbf{R}S(\mathbf{w})\mathbf{R}^T = S(\mathbf{R}\mathbf{w})$  can be obtained

$$\begin{aligned} \dot{\mathbf{R}}_E &= S({}^B\mathbf{w}_E){}^B\mathbf{R}_E = {}^B\dot{\mathbf{R}}_P{}^P\mathbf{R}_E + {}^B\mathbf{R}_P{}^P\dot{\mathbf{R}}_E \\ &= S({}^B\mathbf{w}_P){}^B\mathbf{R}_E + S({}^B\mathbf{R}_P{}^P\mathbf{w}_E){}^B\mathbf{R}_E \end{aligned} \tag{20}$$

According to Equation (20), this can be expressed as

$${}^B\mathbf{w}_E = {}^B\mathbf{w}_P + {}^B\mathbf{R}_P{}^P\mathbf{w}_E \tag{21}$$

$${}^B\mathbf{w}_E = {}^B\mathbf{w}_P + {}^B\mathbf{R}_P\mathbf{J}_{so}\dot{\mathbf{q}} \tag{22}$$

The velocity kinematics model of the hybrid mechanism can be expressed as

$$\dot{\zeta}_e = \begin{bmatrix} {}^B\dot{\mathbf{P}}_E \\ {}^B\mathbf{w}_E \end{bmatrix} = \begin{bmatrix} \mathbf{I} & -S({}^B\mathbf{R}_P{}^P\mathbf{P}_E) \\ \mathbf{0} & \mathbf{I} \end{bmatrix} \begin{bmatrix} {}^B\dot{\mathbf{P}}_P \\ {}^B\mathbf{w}_P \end{bmatrix} + \begin{bmatrix} {}^B\mathbf{R}_P\mathbf{J}_{sp} \\ {}^B\mathbf{R}_P\mathbf{J}_{so} \end{bmatrix} \dot{\mathbf{q}} \tag{23}$$

According to Equations (6), (7) and (23), the Jacobian matrix relationship between the end-effector velocity of the hybrid mechanism relative to the mobile platform velocity of the parallel mechanism and the joint velocity of the serial mechanism is obtained as shown in Equation (24). Compared with the motion range of each leg of the parallel mechanism, the motion range of the mobile platform of the parallel mechanism is more representative of the motion space capability of the parallel mechanism. In this paper, six variables of the platform pose of the parallel mechanism are defined as virtual joints, which together with three joints of the serial mechanism constitute the virtual joints of the hybrid mechanism. Through the motion distribution of the virtual joints of the hybrid mechanism, the motion planning of the joints of the hybrid mechanism is completed. Therefore,  $\mathbf{J}_{task}$  is defined as the Jacobian matrix in the task space of the hybrid mechanism.

$$\dot{\zeta}_e = \begin{bmatrix} {}^B\dot{\mathbf{P}}_E \\ {}^B\mathbf{w}_E \end{bmatrix} = \begin{bmatrix} {}^B\mathbf{R}_P & -S({}^B\mathbf{R}_P{}^P\mathbf{P}_E){}^B\mathbf{R}_P \\ \mathbf{0} & {}^B\mathbf{R}_P \end{bmatrix} \begin{bmatrix} {}^P\dot{\mathbf{P}} \\ \mathbf{w}_P \end{bmatrix} + \begin{bmatrix} {}^B\mathbf{R}_P\mathbf{J}_{sp} \\ {}^B\mathbf{R}_P\mathbf{J}_{so} \end{bmatrix} \dot{\mathbf{q}} \tag{24}$$

$$\dot{\zeta}_e = \mathbf{J}_{task}\dot{\zeta} \tag{25}$$

where  $\mathbf{J}_{task} = \begin{bmatrix} {}^B\mathbf{R}_P & -S({}^B\mathbf{R}_P{}^P\mathbf{P}_E){}^B\mathbf{R}_P & {}^B\mathbf{R}_P\mathbf{J}_{sp} \\ \mathbf{0} & {}^B\mathbf{R}_P & {}^B\mathbf{R}_P\mathbf{J}_{so} \end{bmatrix}$ .

#### 4. Motion Planning Method

##### 4.1. Pseudo-Inverse Method and Weighted Pseudo-Inverse Method

Since the Jacobian matrix of the task space has more columns than rows, it is different from the three-DOF Jacobian matrix inverse solution of the serial mechanism based on the

definition of the generalized inverse. There is a right pseudo-generalized inverse for the nine-DOF Jacobian matrix of the hybrid mechanism, as follows:

$$\dot{\xi} = J_{task}^{\dagger} \dot{\xi}_e \tag{26}$$

where  $J_{task}^{\dagger} = J_{task}^T (J_{task} J_{task}^T)^{-1}$ .

The advantages of the pseudo-inverse method are its simple structure and easy application. The main shortcoming is that the serial and parallel mechanisms are treated equally without considering structural differences.

The hybrid mechanism consists of a parallel mechanism and a serial mechanism, both of which have different advantages. For example, the parallel mechanism has a fast response velocity and compensates simultaneously for a small position range and orientation. Furthermore, the orientation compensation ability is relatively strong, while the serial mechanism has superiority in position space compensation. In summary, the weighted pseudo-inverse method is adopted in coordinate motion for different tasks.

Adding a positive definite weighted matrix  $W$  for motion planning, we introduce transformations  $J_W = J_{task} W^{-1/2}$  and  $\dot{\xi}_W = W^{1/2} \dot{\xi}$  to Equation (26).  $l$  is the weighting index. The larger the  $l$  value, the more pronounced the weighting effect. When  $l = 0$ , there is no weighting effect. Generally, the default value  $l = 1$  is used.  $W^{-1}$  is considered as the motion planning matrix of the hybrid mechanism.

$$\dot{\xi}_e = (J_{task} W^{-l/2}) (W^{l/2} \dot{\xi}) = J_W \dot{\xi}_W \tag{27}$$

Different sea conditions and tasks require corresponding mechanisms to exploit the benefits of their configurations. The weighted pseudo-inverse method is added to the weight  $\beta$  for parallel and serial connections. The larger the  $\beta$  value, the greater the compensation effect of the parallel mechanism, and the smaller the compensation effect of the serial mechanism. The smaller the  $\beta$  value, the more significant the compensation effect of the serial mechanism, and the smaller the compensation effect of the parallel mechanism. The motion of the parallel mechanism and serial mechanism is coordinated by adjusting the weight  $\beta$ . The weighting formula is adjusted as follows:

$$W^{-1} = \begin{bmatrix} \beta \text{diag}(w_1, w_2 \cdots w_6) & \mathbf{0}_{6 \times 3} \\ \mathbf{0}_{3 \times 6} & (1 - \beta) \text{diag}(w_7, w_8, w_9) \end{bmatrix} \tag{28}$$

Among  $w_1, w_2 \cdots w_9 = 1$ , based on the defined transformation  $J_W = J_{task} W^{-1/2}$ ,  $\dot{\xi}_W = W^{1/2} \dot{\xi}$ , and Equation (28), the following can be obtained:

$$\begin{aligned} \dot{\xi} &= W^{-1/2} \dot{\xi}_W = W^{-1/2} J_W^T (J_W J_W^T)^{-1} \dot{\xi}_e \\ &= W^{-1/2} (J_{task} W^{-l/2})^T \left( J_{task} W^{-l/2} (J_{task} W^{-l/2})^T \right)^{-1} \dot{\xi}_e \end{aligned} \tag{29}$$

After simplification, this can be expressed as

$$\dot{\xi} = W^{-l} J_{task}^T (J_{task} W^{-l} J_{task}^T)^{-1} \dot{\xi}_e \tag{30}$$

When  $l = 0$  is selected, the weighted pseudo-inverse  $J_W^{\dagger}$  degenerates to the pseudo-inverse equation (Equation (26)). When  $l = 1$  is selected, the weighted pseudo-inverse  $J_W^{\dagger}$  is expressed as

$$J_W^{\dagger} = W^{-1} J_{task}^T (J_{task} W^{-1} J_{task}^T)^{-1} \tag{31}$$

Therefore, the weighted pseudo-inverse expression of Equation (30) can be described as

$$\dot{\xi} = J_W^{\dagger} \dot{\xi}_e \tag{32}$$

The pseudo-inverse and weighted pseudo-inverse methods have the advantages of a simple structure and fast calculation for the motion planning of the hybrid mechanism. However, the following problems exist in practical application:

1. The pseudo-inverse method is unable to coordinate the motion of parallel and serial mechanisms for different motion compensation tasks. The weighted pseudo-inverse method can only proportionally distribute the parallel and serial mechanisms.
2. The pseudo-inverse method and the weighted pseudo-inverse method cannot avoid the limit of each joint of the parallel mechanism and the serial mechanism after exceeding the limit. The problem of joint movement exceeding the limit will occur.
3. For the analytical solutions, the pseudo-inverse method and the weighted pseudo-inverse method have the problems of overlap compensation and reverse compensation. The velocity values of each virtual joint are obtained by simulation using the pseudo-inverse method and the weighted pseudo-inverse method, as shown in Tables 3 and 4.

**Table 3.** The virtual joint velocity of the hybrid mechanism obtained by the pseudo-inverse method.

Joints	${}^P\dot{P}_x$	${}^P\dot{P}_y$	${}^P\dot{P}_z$	$w_{p_x}$	$w_{p_y}$	$w_{p_z}$	$\dot{q}_1$	$\dot{q}_2$	$\dot{d}_3$
Unit	cm/s	cm/s	cm/s	°/s	°/s	°/s	°/s	°/s	cm/s
Velocity 1	−6.34	−8.89	−5.43	2.80	−3.36	0.45	0.45	−1.31	−2.93
Velocity 2	−7.37	−11.09	−6.28	2.86	−3.45	0.46	0.46	−1.18	−3.40
Velocity 3	−8.30	−13.19	−7.18	2.91	−3.26	0.47	0.47	−1.04	−3.82

**Table 4.** The virtual joint velocity of the hybrid mechanism obtained by the weighted pseudo-inverse ( $\beta = 0.7$ ).

Joints	${}^P\dot{P}_x$	${}^P\dot{P}_y$	${}^P\dot{P}_z$	$w_{p_x}$	$w_{p_y}$	$w_{p_z}$	$\dot{q}_1$	$\dot{q}_2$	$\dot{d}_3$
Unit	cm/s	cm/s	cm/s	°/s	°/s	°/s	°/s	°/s	cm/s
Velocity 1	−6.39	−8.90	−5.48	2.80	−3.66	0.63	0.27	−1.34	−2.72
Velocity 2	−7.44	−11.10	−6.32	2.86	−3.48	0.64	0.28	−1.21	−3.17
Velocity 3	−8.39	−13.21	−7.22	2.90	−3.29	0.65	0.28	−1.07	−3.57

According to Tables 3 and 4, we can draw the following conclusions:

- (a) In the pseudo-inverse simulation, the velocity of the parallel mechanism  $w_{p_z}$  and the velocity of the serial mechanism  $\dot{q}_1$  are in the same direction and have the same value. The velocity direction is the same in the weighted pseudo-inverse simulation, but the value is different. Since the analytical solution cannot consider the configuration, both joints are still simultaneously compensated when the z-directional motion is assigned a small velocity, resulting in overlapping compensation.
- (b) In the simulation of the pseudo-inverse method and weighted pseudo-inverse method, the  $w_{p_y}$  of the parallel mechanism is in the same direction as the  $\dot{q}_2$  of the serial mechanism. The configuration showed that a negative value of  $w_{p_y}$  causes the serial mechanism gangway to move upward and a negative value of  $\dot{q}_2$  causes the serial mechanism gangway to move downward. The current analytic solution causes the reverse motion of joints in the null space.

To solve the above problems, a multi-task redundant hybrid boarding system motion planning method is proposed in this paper.

#### 4.2. MTMP

Since the hybrid mechanism is a redundant degree of freedom configuration, an internal motion exists in null space. This only affects the internal joint motion of the hybrid mechanism, independent of the motion state of the end-effector. The secondary task kinematic equations in null space are added to the weighted pseudo-inverse method, as shown in Equation (33).

$$\dot{\xi} = J_W^+ \dot{\zeta}_e + (I_N - J_W^+ J_W) \dot{\zeta}_a \tag{33}$$

The first term of Equation (33) is the Jacobian matrix for the primary task, and the second term is the Jacobian matrix for the secondary task in null space. Where  $\dot{\zeta}_a = \sum_{i=1}^k \lambda_i J_{ai}^+ \dot{\zeta}_{ai}$ ,  $k$  is the number of secondary tasks;  $\dot{\zeta}_{ai}$  represents the secondary task and  $\lambda_i$  is the weight of the secondary task.  $J_{ai}^+$  is the Jacobian matrix corresponding to the secondary tasks.

To avoid the typical drift caused by the numerical integration of the velocity vector, a closed-loop version of Equation (33) can be adopted in the form [28]

$$\dot{\xi} = J_W^+ (\dot{\zeta}_{de} + k_e e_e) + \lambda_i (I_N - J_W^+ J_W) \left( \sum_{i=1}^k J_{ai}^+ (\dot{\zeta}_{ai} + k_{ai} e_{ai}) \right) \tag{34}$$

where  $e_e = \zeta_{de} - \zeta_{de\_t}$ ,  $e_{ai} = \zeta_{ai} - \zeta_{ai\_t}$ , and  $\zeta_{de}$  are the expected values of the primary task,  $\zeta_{de\_t}$  is the current value of the primary task,  $\zeta_{ai}$  is the expected value of the secondary task,  $\zeta_{ai\_t}$  is the current value of the secondary task, and  $k_e$  and  $k_{ai}$  are the scale factors.

While ensuring the main motion compensation task, the hybrid mechanism must deal with multiple constraints (secondary tasks), such as internal joint reverse compensation, joint limits, etc. The hybrid mechanism needs a motion planning processing method to handle these tasks. A weighted pseudo-inverse coordinated motion control method is proposed with multiple secondary tasks. The main secondary tasks are as follows:

Virtual joint limit: There are different joint limit positions for both parallel and serial mechanisms. Exceeding this limit position will cause damage to the actuator, and the planned motion space posture is impossible to achieve. The parallel mechanism's six-DOF motion and the serial mechanism's three joints are defined as virtual joints of the hybrid mechanism. When planning the motion of the hybrid configuration, it is necessary to ensure that the movement is within the limit position of the virtual joints of the hybrid mechanism. The objective optimization function defined in the literature is used [29], as shown in Equation (35).

$$H(q) = \sum_{i=1}^n \frac{(q_{i,max} - q_{i,min})^2}{c_i (q_{i,max} - q_i) (q_i - q_{i,max})} \tag{35}$$

where  $q_{i,max}$  and  $q_{i,min}$  are the upper and lower limits of the corresponding virtual joint degrees of freedom,  $c_i$  is a constant factor, and  $n$  is the number of virtual joint degrees of freedom to be restricted. The derivative of the objective function  $q_i$  with respect to the variable  $H(q)$  is obtained

$$\frac{\partial H}{\partial q_i} = \frac{(q_{i,max} - q_{i,min})^2 (2q_i - q_{i,max} - q_{i,min})}{c_i (q_{i,max} - q_i) (q_i - q_{i,min})}, i = 1, 2 \dots n \tag{36}$$

Then, the weight of Equation (28) can be redefined as

$$W^{-1} = \begin{bmatrix} \beta \text{diag}(w_1, w_2 \dots w_6) & \mathbf{0}_{6 \times 3} \\ \mathbf{0}_{3 \times 6} & (1 - \beta) \text{diag}(w_7, w_8, k_c w_9) \end{bmatrix} \tag{37}$$

where  $w_i = \frac{1}{1 + \left| \frac{\partial H}{\partial q_i} \right|}, i = 1, 2 \dots n$ .

From Equations (36) and (37), it can be seen that when the virtual joint angle of the hybrid mechanism is at the middle of the upper and lower limits,  $w_i = 1$ . When the joint angle of the hybrid mechanism approaches the upper or lower limits,  $w_i$  tends to 0, thus ensuring that the movement of each joint angle of the hybrid mechanism is within the limit. Since the motion range of the telescopic joint of the serial mechanism is relatively large, an amplification coefficient  $k_c$  is added. The weight coefficient of the joint is defined as  $k_c w_9$ .

Secondary task 1: The  $w_{p_z}$  of the parallel mechanism and the  $\dot{q}_1$  of the first joint of the serial mechanism are optimized twice. This task is carried out to reduce internal energy consumption, to prevent low-velocity jitter, and to increase the rigidity of the parallel mechanism.

By configuration analysis, it can be seen that the rotation of  $w_{p_z}$  of the parallel mechanism and  $\dot{q}_1$  of the first joint of the serial mechanism have the same effect on the hybrid mechanism end. Since the pseudo-inverse method is a numerical analysis, the advantages and disadvantages of the configurations are not considered in the solution process. When the rotation velocity is low or the angle is small, the results of the pseudo-inverse method and the weighted pseudo-inverse method still require double-joint motion compensation. By increasing the overall internal movement and energy consumption, it is also easy to cause low-speed jitter. Due to the characteristics of the parallel mechanism, its z-direction offset angle is limited, and excessive deflection reduces the rigidity of the parallel mechanism. Considering the configuration characteristics of both joints, an internal joint velocity optimization algorithm is proposed, where the first joint of the serial mechanism is used as the primary compensation task in this direction. The z-axis rotation direction of the mobile platform on the parallel mechanism is used as the auxiliary compensation task.

The secondary task 1 Jacobian matrix can be written as

$$J_{a1} = \begin{bmatrix} 0 & 0 & 0 & 0 & 0 & 1 & 0 & 0 & 0 \\ 0 & 0 & 0 & 0 & 0 & 0 & 1 & 0 & 0 \end{bmatrix} \tag{38}$$

The maximum positive offset angle of the first joint of the serial mechanism is defined as  $q_{1,max}$ , the maximum negative offset angle is defined as  $q_{1,min}$ , the maximum positive velocity is defined as  $\dot{q}_{1,max}$ , the maximum negative velocity is defined as  $-\dot{q}_{1,max}$ , and the critical protection angle is defined as  $\sigma$ .  $q_{1,min} + \sigma < q_1 < q_{1,max} - \sigma$  is the flexible compensation range of the first joint of the serial mechanism.  $q_1$  is to be operated in this range before the hybrid mechanism starts motion compensation.

The sum of  $\dot{q}_1$  of the serial mechanism and  $w_{p_z}$  of the parallel mechanism is  $w_{1sum}$ . When the first joint of the serial mechanism is operated within the critical protection angle range,  $w_{1sum}$  cannot exceed the maximum value of  $\dot{q}_{1,max}$ , as this may cause the joint to exceed the angle limit.

The internal joint velocity optimization algorithm of secondary task 1 is implemented as Algorithm 1.

---

**Algorithm 1** Internal joint velocity optimization

---

- 1: **if**  $q_{1,min} + \sigma \leq q_1 \leq q_{1,max} - \sigma$  **then**
  - 2:     **if**  $-\dot{q}_{1,max} < w_{1sum} < \dot{q}_{1,max}$  **then**
  - 3:          $\dot{q}_1 = w_{1sum}, w_{p_z} = 0$
  - 4:     **else if**  $w_{1sum} > \dot{q}_{1,max}$  **then**
  - 5:          $\dot{q}_1 = \dot{q}_{1,max}, w_{p_z} = w_{1sum} - \dot{q}_{1,max}$
  - 6:     **else if**  $w_{1sum} < -\dot{q}_{1,max}$  **then**
  - 7:          $\dot{q}_1 = -\dot{q}_{1,max}, w_{p_z} = w_{1sum} + \dot{q}_{1,max}$
  - 8: **else if**  $q_{1,min} < q_1 < q_{1,min} + \sigma$  **then**
  - 9:      $\dot{q}_1 = \frac{1}{2} \cdot w_{1sum} \cdot [1 + \cos(\frac{q_{1,min} + \sigma - q_1}{\sigma} \pi)], w_{p_z} = \frac{1}{2} \cdot w_{1sum} \cdot [1 - \cos(\frac{q_{1,min} + \sigma - q_1}{\sigma} \pi)]$
  - 10: **else if**  $q_{1,max} - \sigma < q_1 < q_{1,max}$  **then**
  - 11:      $\dot{q}_1 = \frac{1}{2} \cdot w_{1sum} \cdot [1 + \cos(\frac{q_1 - q_{1,max} + \sigma}{\sigma} \pi)], w_{p_z} = \frac{1}{2} \cdot w_{1sum} \cdot [1 - \cos(\frac{q_1 - q_{1,max} + \sigma}{\sigma} \pi)]$
  - 12: **else if**  $q_1 < q_{1,min}$  **or**  $q_1 > q_{1,max}$  **then**
  - 13:      $w_{p_z} = w_{1sum}, \dot{q}_1 = 0$
- 

Since secondary task 1 solves the problem of overlapping internal joint motions according to the configuration characteristics, it can be mapped in the null space or processed during the velocity distribution.

Secondary task 2: The angle and velocity of the second joint of the serial mechanism are optimized, the problem of internal joint reverse compensation is solved, and the torque pressure of the single joint of the serial mechanism is reduced.

Due to configuration reasons, the analytical solutions of the pseudo-inverse method and the weighted pseudo-inverse method experience reverse compensation motion between the pose movement of the parallel mechanism and the second joint motion of the serial mechanism. The second joint of the serial mechanism has to carry the weight of the gangway and requires a wide range of orientation compensation, which generates a larger torque. The pressure is large for a single joint.

Therefore, a secondary task is added to the zero space using the gradient descent method to make the angle approach the fixed angle of the initial compensation task and the velocity approach zero. When the parallel mechanism exceeds the compensation range, the second joint's compensation range of the serial mechanism will increase.

$$J_{a2} = [ 0 \ 0 \ 0 \ 0 \ 0 \ 0 \ 0 \ 0 \ 1 \ 0 ] \tag{39}$$

$$\zeta_{a2} = \tilde{q}_2 \tag{40}$$

where  $\zeta_{a2}$  is the target motion change in the serial mechanism's second joint and  $\tilde{q}_2$  is the initial angle of  $q_2$  after the end of the hybrid mechanism reaches the target point.

### 5. Simulation Analysis

#### 5.1. Simulation Initial Conditions and Parameter Settings

In inertial space, the target point at the end of the hybrid mechanism is in a fixed position, such as a wind turbine tower. To accurately measure the trajectory of the hybrid mechanism, which needs motion compensation, the sensor is installed at the base of the hybrid mechanism. There is an unavoidable delay due to the hydraulic drive of the joints of the hybrid mechanism and the response delay of the controller. The motion trajectory of the hybrid mechanism is predicted by the change data of the pose trajectory collected by the sensor, and its acting position is the origin of the sensor frame. The direction of motion compensation of the hybrid mechanism is opposite to the position and orientation measured by the sensor.

When the hybrid mechanism starts preparing for wave motion compensation, the parallel mechanism moves to the neutral position with the maximum range of motion compensation space or a height close to the target point. After the parallel mechanism runs to the neutral position, the end of the serial mechanism is manually operated to the designated position. When the end-effector of the hybrid mechanism reaches the target position, it enters an active compensation operation state.

In the current motion compensation operating state of the hybrid mechanism, the mobile platform of the parallel mechanism rises 0.95 m relative to the initial state, and the gangway of the serial platform remains parallel to the horizontal plane and extends 3.5 m. The mechanism parameters are shown in Table 5.

**Table 5.** Hybrid mechanism parameters.

Mechanism	Joints	Initial State	Active Compensation Operating State
Parallel mechanism	$l_1, l_2, l_3, l_4, l_5, l_6$	2.58 m	3.234 m
	$x_p, y_p, z_p$	(0,0,1.525) m	(0,0,2.475) m
	$\phi_p, \theta_p, \psi_p$	(0,0,0) <sup>o</sup>	(0,0,0) <sup>o</sup>
Serial mechanism	$q_1$	0 <sup>o</sup>	0 <sup>o</sup>
	$q_2$	0 <sup>o</sup>	0 <sup>o</sup>
	$d_3$	9.552 m	13.052 m

During the joint movement of the hybrid mechanism, it is necessary to ensure that the internal virtual joints do not exceed their maximum range of motion. Otherwise, the

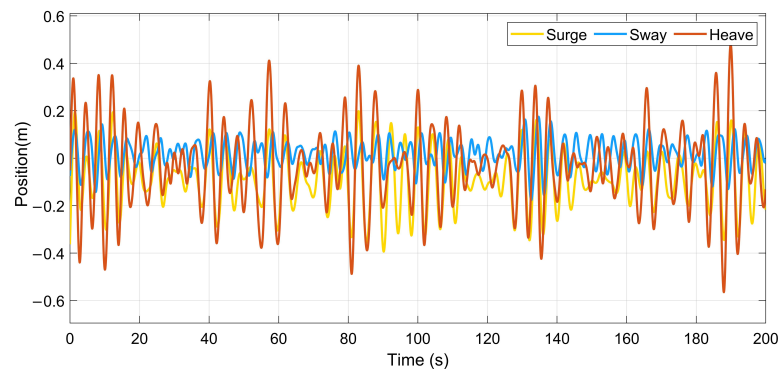
driving devices will be damaged, and the end posture will not reach the specified target point. The maximum telescopic range of the parallel mechanism legs is 1.6 m, and the maximum telescopic range of the gangway is 7 m. Table 6 shows the limit variation range of each virtual joint in the working state of the hybrid mechanism.

**Table 6.** Virtual joint limit range in working conditions.

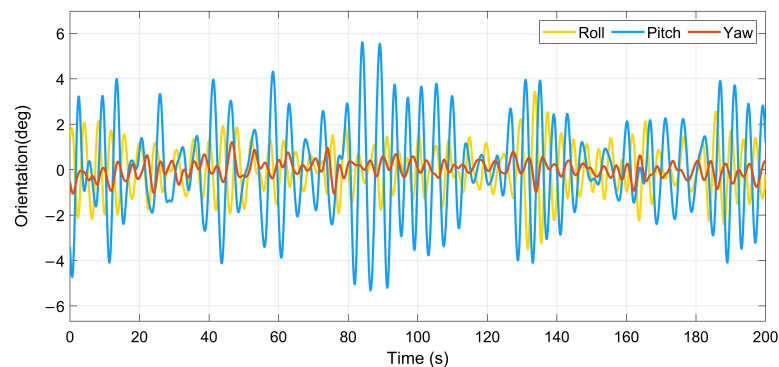
Mechanism	Joints	Max.	Min.
Parallel mechanism	$x_p$	1.165 m	−1.36 m
	$y_p$	1.15 m	−1.15 m
	$z_p$	1.12 m	−0.95 m
	$\phi_p$	30°	−30°
	$\theta_p$	30°	−30°
	$\psi_p$	36°	−36°
Serial mechanism	$q_1$	30°	−30°
	$q_2$	30°	−30°
	$d_3$	3.5 m	−3.5 m

5.2. Simulation and Comparison

According to the motion characteristics of the vessel during the boarding operation, the change trajectory of the base frame of the hybrid mechanism caused by the wave motion in the sensor coordinate system is randomly simulated, with a duration of 200 s. Six of these variables are surge, sway, heave, roll, pitch, and yaw as input trajectories, as shown in Figure 8.



(a) Position trajectory



(b) Orientation trajectory

**Figure 8.** Motion trajectory of the hybrid mechanism’s base platform caused by waves.

The motion trajectory of the base of the hybrid mechanism caused by the wave motion is input into the pseudo-inverse method, weighted pseudo-inverse method, and MTMP method for simulation.

1. The pseudo-inverse method is used to coordinate the motion of the hybrid mechanism. The deviation coefficient  $k_e$  is 25. Through simulation, the displacements of the legs of the parallel mechanism and the joints of the serial mechanism can be obtained, as shown in Figures 9 and 10.

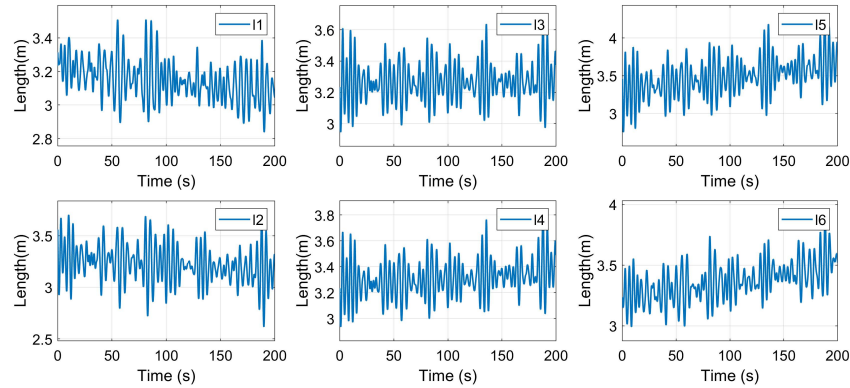


Figure 9. Parallel mechanism leg displacement in the pseudo-inverse method.

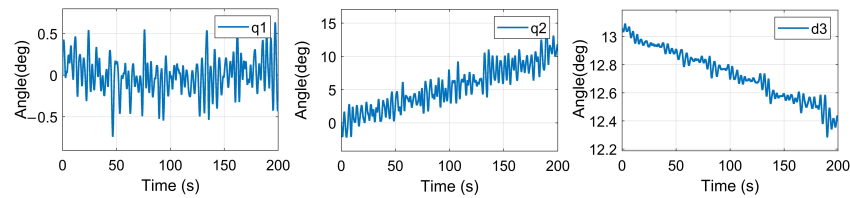


Figure 10. Serial mechanism joint displacement in the pseudo-inverse method.

2. The weighted pseudo-inverse method is used for the wave compensation of the hybrid mechanism. The deviation coefficient adopts the same  $k_e$  as the pseudo-inverse method, at 25. Since the parallel mechanism is a flexible mechanism with full degrees of freedom in the hybrid mechanism, the distribution coefficient is usually higher than that of the serial mechanism; as a result, the weighted allocation factor  $\beta$  is 0.7. The simulation results obtained are shown in Figures 11 and 12.

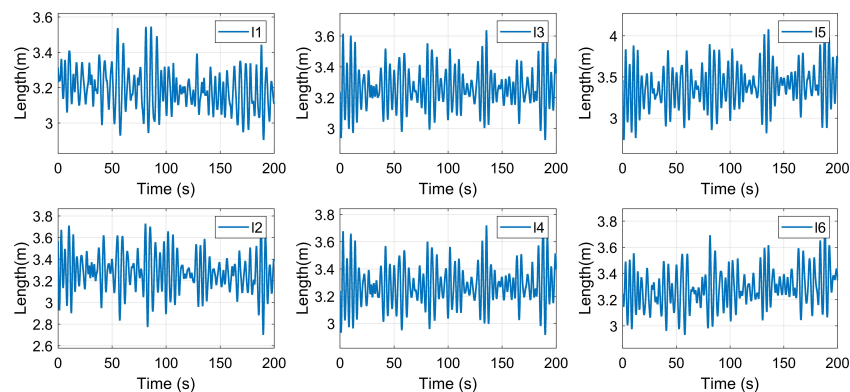


Figure 11. Parallel mechanism leg displacement in the weighted pseudo-inverse method.

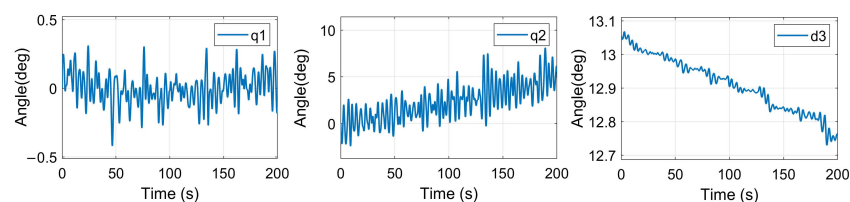


Figure 12. Serial mechanism joint displacement in the weighted pseudo-inverse method.

- The MTMP method is used for the hybrid mechanism of sea wave compensation. The coefficients are the same as the weighted pseudo-inverse method. When the  $k_e$  factor is 25, the weighted allocation factor  $\beta$  is 0.7, and the  $k_c$  factor is 9. Considering the virtual joint limit, for secondary task 1 and secondary task 2, the obtained simulation results are shown in Figures 13 and 14.

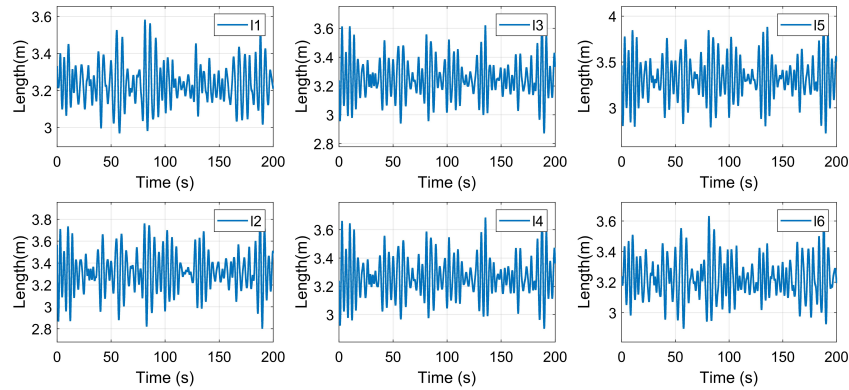


Figure 13. Parallel mechanism leg displacement in the MTMP method.

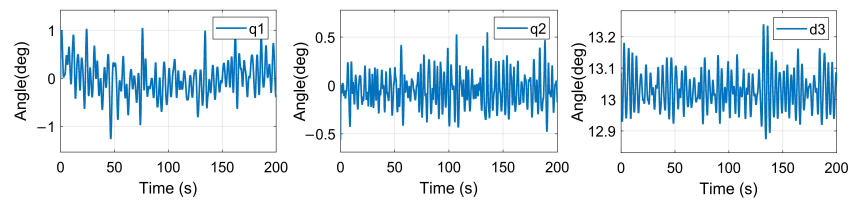


Figure 14. Serial mechanism joint displacement in the MTMP method.

The motion trajectory of the hybrid mechanism’s base platform caused by waves and the compensation trajectory of the base platform after motion planning using the MTMP method are shown in Figure 15.

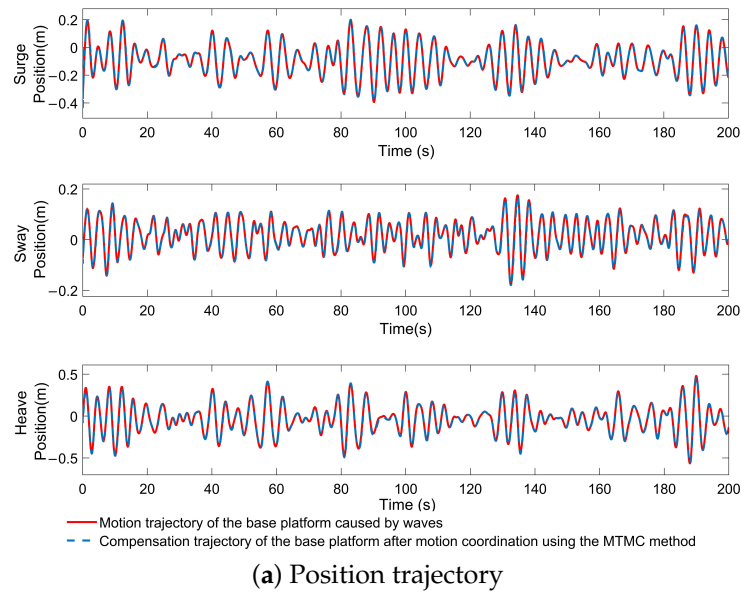
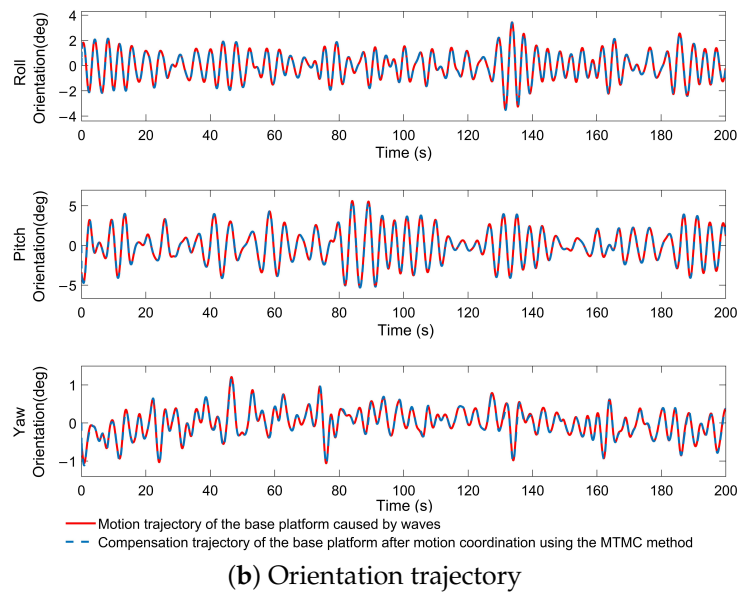


Figure 15. Cont.



**Figure 15.** The motion trajectory of the hybrid mechanism’s base platform caused by waves and the compensation trajectory of the base platform after motion planning using the MTMP method.

5.3. Simulation Result Analysis

A simulation comparison is conducted for the pseudo-inverse method, weighted pseudo-inverse method, and MTMP method.

Simulation result analysis 1: Figures 8–15 show that the joint values of the pseudo-inverse and weighted pseudo-inverse methods will diverge with time, where  $l_1, l_2, l_5, l_6, q_2,$  and  $d_3$  are more prominent. The joints of the MTMP method follow time change convergence. The  $d_3$  of the serial mechanism in the pseudo-inverse method and the weighted pseudo-inverse method compensates for a relatively small change in motion. The MTMP method can take advantage of the ability of  $d_3$  to compensate over a larger range.

Simulation result analysis 2: For a simulation of 200 s, the fundamental sample time is 0.05 s, and there are 4000 data points in total. Considering the deviation of the initial integration caused by the difference in the initial value and the trajectory input value at the beginning of the simulation, the first 10 data points are removed. The data during the compensation of the stable motion of the hybrid joint mechanism are analyzed. The maximum and minimum values of the internal joints of the three motion planning methods of the hybrid mechanism during the 200 s simulation can be obtained, as shown in Table 7.

**Table 7.** The maximum and minimum values of the internal joint motion planning process of the three methods of the hybrid mechanism, for the same trajectory input in the 200 s simulation process.

Method	Serial Mechanism			Parallel Mechanism
	$q_1$	$q_2$	$d_3$	$l_1, l_2, l_3, l_4, l_5, l_6$
Pseudo-inverse joints maximum	0.63°	14.93°	13.075 m	4.243 m
Pseudo-inverse joints minimum	−0.73°	−2.11°	12.403 m	2.616 m
Weighted pseudo-inverse joints maximum	0.31°	8.11°	13.068 m	4.102 m
Weighted pseudo-inverse joints minimum	−0.42°	−2.44°	12.729 m	2.707 m
MTMP joints maximum	1.04°	0.54°	13.238 m	3.953 m
MTMP joints minimum	−1.25°	−0.47°	12.876 m	2.729 m

From Table 7, it can be seen that for the MTMP method, each joint motion range is within its limits, preventing the pseudo-inverse method and weighted pseudo-inverse method from exceeding the joint movement range. In the motion compensation process, the maximum value of the legs of the pseudo-inverse parallel mechanism is 4.243 m,

which exceeds its motion range of 2.58 m to 4.18 m. The maximum value of the weighted pseudo-inverse also approaches its critical value.

The MTMP method is compared with the pseudo-inverse method and the weighted pseudo-inverse method. The maximum and minimum values of the nine variables in the hybrid mechanism have greater margins.

Simulation result analysis 3: According to Figure 15, the input compensation trajectory is consistent with the trajectory after the motion distribution. Combining the results of analyses 1 and 2 shows that the MTMP method can accurately realize the trajectory tracking of the primary task. While exerting the motion constraints of multiple secondary tasks, this does not affect the end trajectory.

## 6. Conclusions

Reasonable motion planning is essential for the safe operation of a nine-DOF redundant hybrid boarding system. The MTMP method proposed in this paper is based on the internal configuration characteristics. Under stable tracking of the primary task trajectory, the virtual joint limit and two internal joint velocity optimization tasks are used to constrain the joint motion. Through a simulation comparison with a pseudo-inverse method and weighted pseudo-inverse method, the following findings regarding the use of the MTMP method for the redundant hybrid boarding system are obtained: 1. The motion change in each joint of the hybrid mechanism is relatively convergent with time. Furthermore, this method can exploit the compensation ability of different dominant joints. 2. The MTMP method ensures that the joints of the hybrid mechanism perform motion compensation within their limited range of motion. 3. By optimizing the internal joint velocity of the hybrid mechanism, the overlap compensation and reverse compensation of the pseudo-inverse method and the weighted pseudo-inverse method analytical solution are solved, and the rigidity of the parallel mechanism is enhanced. The MTMP motion planning method is designed to obtain a more extensive margin of motion for the hybrid mechanism's joints and to increase the hybrid mechanism's range of motion in terms of compensation space.

**Author Contributions:** Conceptualization, methodology and software, Y.W. (Yueyue Wang) and W.G.; writing—original draft preparation, Y.W. (Yueyue Wang); writing—review and editing, Y.W. (Yueyue Wang), W.G. and Y.W. (Yanhui Wei); supervision, Y.W. (Yanhui Wei); funding acquisition, Y.W. (Yanhui Wei) and Y.H.; validation, Y.W. (Yanhui Wei) and T.M. All authors have read and agreed to the published version of the manuscript.

**Funding:** This work was financially supported by the Key Research and Development Program of the Ministry of Science and Technology (2020YFC1512200), the general project of Hainan Natural Science Foundation (622MS163), and the joint project of scientific and technological innovation in Hainan Province (2021CXLH0001).

**Institutional Review Board Statement:** Not applicable.

**Informed Consent Statement:** Not applicable.

**Data Availability Statement:** Not applicable.

**Conflicts of Interest:** The authors declare no conflict of interest.

## References

1. IRENA. *Offshore Renewables: An Action Agenda for Deployment*; International Renewable Energy Agency: Abu Dhabi, United Arab Emirates, 2021.
2. Hu, B.; Stumpf, P.; van der Deijl, W. *Offshore Wind Access 2019*; TNO Report; TNO: Petten, The Netherlands, 2019; pp. 1–40.
3. Kang, J.; Sobral, J.; Soares, C.G. Review of condition-based maintenance strategies for offshore wind energy. *J. Mar. Sci. Appl.* **2019**, *18*, 1–16. [[CrossRef](#)]
4. Liu, X.; Li, W.; Wang, W.; Xu, Z. Control for the new harsh sea conditions salvage crane based on modified fuzzy pid. *Asian J. Control* **2018**, *20*, 1582–1594. [[CrossRef](#)]
5. Ngo, Q.; Nguyen, N.; Nguyen, C.; Tran, T.; Bui, V. Payload pendulation and position control systems for an offshore container crane with adaptive-gain sliding mode control. *Asian J. Control* **2020**, *22*, 2119–2128. [[CrossRef](#)]

6. Chen, H.; Xie, J.; Han, J.; Shi, W.; Charpentier, J.-F.; Benbouzid, M. Position Control of Heave Compensation for Offshore Cranes Based on a Particle Swarm Optimized Model Predictive Trajectory Path Controller. *J. Mar. Sci. Eng.* **2022**, *10*, 1427. [[CrossRef](#)]
7. Gangways. Available online: <https://www.smstequipment.com/offshore-access/gangways/> (accessed on 24 October 2021).
8. Chen, B.Y.; Chiang, M.H. Simulation and experiment of a turbine access system with three-axial active motion compensation. *Ocean Eng.* **2019**, *176*, 8–19. [[CrossRef](#)]
9. Li, E.; Zhao, T.; Wang, C.; Wang, W.; Bian, H. Mechanism Modeling of Sea Motion Compensated Hybrid Gangway. *Ship Eng.* **2018**, *40*, 66–72.
10. Liang, L.; Le, Z.; Zhang, S.; Li, J. Modeling and controller design of an active motion compensated gangway based on inverse dynamics in joint space. *Ocean Eng.* **2020**, *197*, 106864. [[CrossRef](#)]
11. Cai, Y.; Zheng, S.; Liu, W.; Qu, Z.; Han, J. Model Analysis and Modified Control Method of Ship-Mounted Stewart Platforms for Wave Compensation. *IEEE Access* **2020**, *9*, 4505–4517. [[CrossRef](#)]
12. Sun, M.; Wang, S.; Han, G.; An, L.; Chen, H.; Sun, Y. Modeling and Dynamic Analysis of a Triple-Tagline Anti-Swing System for Marine Cranes in an Offshore Environment. *J. Mar. Sci. Eng.* **2022**, *10*, 1146. [[CrossRef](#)]
13. Sun, P.; Li, Y.B.; Wang, Z.S.; Chen, K.; Yue, Y. Inverse displacement analysis of a novel hybrid humanoid robotic arm. *Mech. Mach. Theory* **2020**, *147*, 103743. [[CrossRef](#)]
14. Su, H.; Hu, Y.; Karimi, H.R.; Knoll, A. Ferrigno, G.; DeMomi, E. Improved recurrent neural network-based manipulator control with remote center of motion constraints: Experimental results. *Neural Netw.* **2020**, *131*, 291–299. [[CrossRef](#)] [[PubMed](#)]
15. Zhang, Z.; Chen, S.; Li, S. Compatible Convex-Nonconvex Constrained QP-Based Dual Neural Networks for Motion Planning of Redundant Robot Manipulators. *IEEE Trans. Control Syst.* **2019**, *27*, 1250–1258. [[CrossRef](#)]
16. Zhang, Z.; Yan, Z. A Varying Parameter Recurrent Neural Network for Solving Nonrepetitive Motion Problems of Redundant Robot Manipulators. *IEEE Trans. Control Syst.* **2019**, *27*, 2680–2687. [[CrossRef](#)]
17. Wang, Z.; Li, Y.; Sun, P.; Luo, Y.; Chen, B.; Zhu, W. A multi-objective approach for the trajectory planning of a 7-DOF serial-parallel hybrid humanoid arm. *Mech. Mach. Theory* **2021**, *165*, 104423. [[CrossRef](#)]
18. Peng, J.; Xu, W.; Liu, T.; Yuan, H.; Liang, B. End-effector pose and arm-shape synchronous planning methods of a hyper-redundant manipulator for spacecraft repairing. *Mech. Mach. Theory* **2021**, *155*, 104062. [[CrossRef](#)]
19. Lee, W.; Lee, Y.; Park, G.; Hong, S.; Kang, Y. A whole-body rescue motion control with task-priority strategy for a rescue robot. *Auton. Robots* **2017**, *41*, 243–258. [[CrossRef](#)]
20. Li, B. Effect of hydrodynamic coupling of floating offshore wind turbine and offshore support vessel. *Appl. Ocean Res.* **2021**, *114*, 102707. [[CrossRef](#)]
21. Ding, B.; Cazzolato, B.S.; Grainger, S.; Stanley, R.M.; Costi, J.J. Active preload control of a redundantly actuated Stewart platform for backlash prevention. *Robot. Comput. Integr. Manuf.* **2015**, *32*, 11–24. [[CrossRef](#)]
22. Hou, Y.; Zhang, G.; Zeng, D. An efficient method for the dynamic modeling and analysis of Stewart parallel manipulator based on the screw theory. *Proc. Inst. Mech. Eng. Part C J. Mech. Eng. Sci.* **2020**, *234*, 808–821. [[CrossRef](#)]
23. Qiao, D.; Zhi, G.; Yan, J. Active truncation model test method of deep-water mooring system: A numerical simulation study on time delay compensation of actuator motion. *Appl. Ocean Res.* **2021**, *111*, 102645. [[CrossRef](#)]
24. Wei, Y.; Wang, A.; Han, H. Ocean wave active compensation analysis of inverse kinematics for hybrid boarding system based on fuzzy algorithm. *Ocean Eng.* **2019**, *182*, 577–583. [[CrossRef](#)]
25. Kumar, S.; WWöhrle, H.; de Gea Fernández, J.; Müller, A.; Kirchner, F. A survey on modularity and distributivity in series-parallel hybrid robots. *Mechatronics* **2020**, *68*, 102367. [[CrossRef](#)]
26. Veremey, E.; Sotnikova, M. Optimal filtering correction for marine dynamical positioning control system. *J. Mar. Sci. Appl.* **2016**, *15*, 452–462. [[CrossRef](#)]
27. Craig, J.J. *Introduction to Robotics*, 4th ed.; Addison Wesley: Boston, MA, USA, 2018.
28. Antonelli, G.; Chiaverini, S. Task-priority redundancy resolution for underwater vehicle-manipulator systems. In Proceedings of the IEEE International Conference on Robotics and Automation, Leuven, Belgium, 20 May 1998; Volume 1, pp. 768–773.
29. Chan, T.F.; Dubey, R.V. A weighted least-norm solution based scheme for avoiding joint limits for redundant joint manipulators. *IEEE Trans Rob Autom.* **1995**, *11*, 286–292. [[CrossRef](#)]

**Disclaimer/Publisher’s Note:** The statements, opinions and data contained in all publications are solely those of the individual author(s) and contributor(s) and not of MDPI and/or the editor(s). MDPI and/or the editor(s) disclaim responsibility for any injury to people or property resulting from any ideas, methods, instructions or products referred to in the content.